



**HAL**  
open science

## 12 CO<sub>2</sub> transition frequencies with kHz-accuracy by saturation spectroscopy in the 1.99–2.09 $\mu\text{m}$ region

H. Fleurbaey, P. Čermák, A. Campargue, S. Kassi, D. Romanini, O. Votava,  
D. Mondelain

### ► To cite this version:

H. Fleurbaey, P. Čermák, A. Campargue, S. Kassi, D. Romanini, et al.. 12 CO<sub>2</sub> transition frequencies with kHz-accuracy by saturation spectroscopy in the 1.99–2.09  $\mu\text{m}$  region. *Physical Chemistry Chemical Physics*, 2023, 25 (24), pp.16319-16330. 10.1039/d3cp01603j . hal-04221903

**HAL Id: hal-04221903**

**<https://hal.science/hal-04221903>**

Submitted on 16 Nov 2023

**HAL** is a multi-disciplinary open access archive for the deposit and dissemination of scientific research documents, whether they are published or not. The documents may come from teaching and research institutions in France or abroad, or from public or private research centers.

L'archive ouverte pluridisciplinaire **HAL**, est destinée au dépôt et à la diffusion de documents scientifiques de niveau recherche, publiés ou non, émanant des établissements d'enseignement et de recherche français ou étrangers, des laboratoires publics ou privés.

1  $^{12}\text{CO}_2$  transition frequencies with kHz-accuracy  
2 by saturation spectroscopy in the 1.99-2.09  $\mu\text{m}$  region  
3

4 H. Fleurbaey<sup>1</sup>, P. Čermák<sup>1,2</sup>, A. Campargue<sup>1</sup>, S. Kassi<sup>1</sup>, D. Romanini<sup>1</sup>, O. Votava<sup>1,3</sup>, D. Mondelain<sup>1\*</sup>  
5

6 <sup>1</sup>*Univ. Grenoble Alpes, CNRS, LIPhy, 38000 Grenoble, France*

7 <sup>2</sup>*Department of Experimental Physics, Faculty of Mathematics, Physics and Informatics, Comenius*  
8 *University, Mlynská Dolina, 842 48 Bratislava, Slovakia*

9 <sup>3</sup>*J. Heyrovský Institute of Physical Chemistry, ASCR, Dolejškova 3, Prague 8, Czech Republic*  
10

11  
12  
13  
14 \*Corresponding author: [didier.mondelain@univ-grenoble-alpes.fr](mailto:didier.mondelain@univ-grenoble-alpes.fr); LIPhy, Bat. E, 140 rue de la  
15 Physique, 38400 Saint-Martin d'Hères (France).  
16  
17  
18  
19  
20  
21  
22  
23

24 **Key words**

25 Frequency measurements; carbon dioxide; saturation spectroscopy; CRDS; coherence transfer  
26

27        **Abstract**

28        Saturation spectroscopy has been used to determine absolute frequencies of 107 ro-vibrational  
29 transitions of the two strongest  $^{12}\text{CO}_2$  bands of the 2  $\mu\text{m}$  region. The considered 20012-00001 and  
30 20013-00001 bands are of importance for the  $\text{CO}_2$  monitoring in our atmosphere. Lamb dips were  
31 measured using a cavity ring-down spectrometer linked to an optical frequency comb referenced to a  
32 GPS-disciplined Rb oscillator or to an ultra-stable optical frequency. The comb-coherence transfer  
33 (CCT) technique was applied to obtain a RF tunable narrow-line laser comb-disciplined source using  
34 an external cavity diode laser and a simple electro-optic modulator. This setup allows obtaining  
35 transition frequency measurements with kHz-level accuracy. The resulting accurate values of the  
36 energy levels of the 20012 and 20013 vibrational states are reproduced with a  $(1\sigma)$ -rms of about 1  
37 kHz using the standard polynomial model. The two upper vibrational states appear thus to be highly  
38 isolated except for a local perturbation of the 20012 state leading to an energy shift of 15 kHz at  $J=$   
39 43. A recommended list of 145 transition frequencies with kHz accuracy is obtained providing  
40 secondary frequency standards across the 1.99-2.09  $\mu\text{m}$  range. The reported frequencies will be  
41 valuable to constrain the zero-pressure frequencies of the considered transitions in  $^{12}\text{CO}_2$  retrieval  
42 from atmospheric spectra.

43

44

## 1. Introduction

45

46

47

48

49

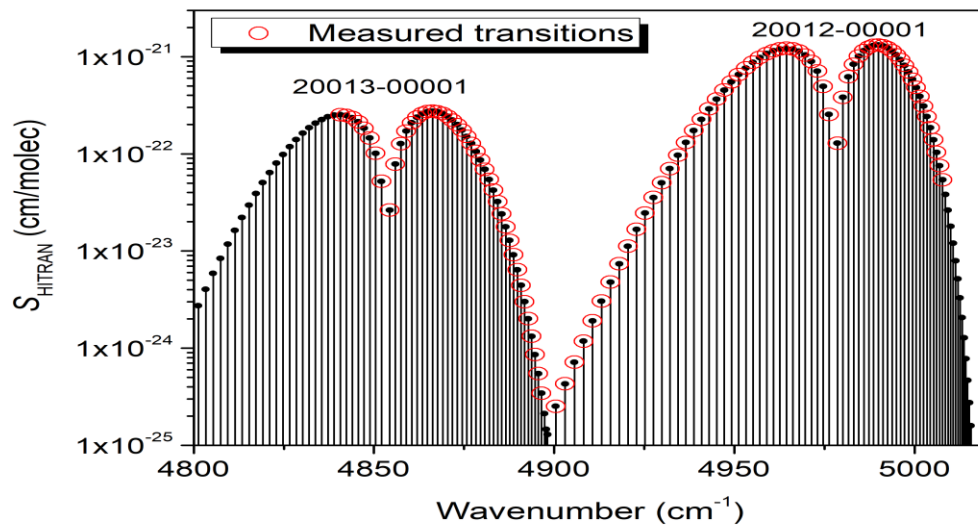
50

51

52

53

Carbon dioxide, CO<sub>2</sub>, is the most important anthropogenic greenhouse gas and several satellite missions like GOSAT, GOSAT-2 (JAXA), OCO-2 (NASA), TanSat (CAS), and the upcoming MicroCarb (CNES) and CO2M (ESA) missions, as well as ground-based networks like TCCON<sup>1</sup>, are dedicated to the monitoring of its column-averaged dry-air mole fraction in the Earth's atmosphere. These missions are increasingly demanding in terms of high quality spectroscopic data for the CO<sub>2</sub> absorption bands in the 1.6 and 2.0 μm regions used for these measurements. In the former spectral region, numerous line profile studies<sup>2,3,4,5,6</sup> as well as highly accurate frequency measurements<sup>7,8,9,10,11,12,13,14</sup> have been reported so far. In particular, transition frequencies with kHz-accuracy were determined both in the Doppler limited regime<sup>8,9,12,13</sup> and in the saturation regime<sup>10,14</sup>.



54

55

56

57

**Fig. 1.** Overview of the 20012-00001 and 20013-00001 bands of <sup>12</sup>CO<sub>2</sub> as provided by the HITRAN database. Transitions presently measured by saturation spectroscopy are highlighted (red open circles).

58

59

60

61

62

63

64

65

66

67

The 2 μm region is dominated by the 20013-00001 and 20012-00001 bands of <sup>12</sup>CO<sub>2</sub> centered at 2.06 and 2.01 μm, respectively (**Fig. 1**). Here we adopt the HITRAN convention for the vibrational labelling (so-called AFGL notation) described in Rothman and Young<sup>15</sup>. These bands have been the subject of several spectroscopic studies using Fourier transform spectroscopy (FTS)<sup>16,17,18,19,20,21,22,23</sup>, laser diode absorption spectroscopy<sup>24,25,26,27,28,29</sup> and cavity ring down spectroscopy (CRDS)<sup>30,31,32</sup>. In particular, the latter CRDS studies were dedicated to accurate measurements of the line profiles broadened by air (and their temperature dependence) in support of missions devoted to CO<sub>2</sub> atmospheric retrieval. Regarding transition frequencies, to the best of our knowledge, only the very recent (zero-pressure) frequencies reported with 100 kHz accuracy for four lines measured by CRDS of CO<sub>2</sub> in air were referenced to an absolute frequency standard<sup>32</sup>. Let us also mention that the

68 absolute positions of five lines of the 21113-01101 band were reported with 300 kHz accuracy in the  
69 2.09  $\mu\text{m}$  spectral region<sup>33</sup>. However, these latter measurements were performed only at 13.3 mbar  
70 (of pure  $\text{CO}_2$ ) and transition frequencies (i.e. line centre at zero-pressure) could not be provided.

71 We report here the frequencies of most of the strongest transitions of the 20013-00001 and  
72 20012-00001 bands with kHz-level accuracy. This provides a series of secondary frequency standards  
73 with kHz-level uncertainties across the wide 4788-5015  $\text{cm}^{-1}$  frequency range (i.e. 1994-2089 nm)  
74 where frequency standards are scarce<sup>7</sup>. Carbon dioxide, a non-toxic and easy-to-manipulate gas with  
75 regularly spaced strong (up to  $10^{-21}$  cm/molecule) transitions, is particularly well adapted for that  
76 purpose. The achieved uncertainty will be valuable for fixing the positions at pressure equal to zero  
77 in the multi-spectrum fit procedures used to analyze spectra of  $\text{CO}_2$  diluted in air, allowing for the  
78 improvement of the other line profile parameters, especially the pressure-shift coefficients (see *e.g.*  
79 Mondelain *et al.*<sup>4</sup>). The obtained frequency values will be also valuable for spectra calibration  
80 purposes as for instance for frequency referencing differential absorption LIDAR (Light Detecting And  
81 Ranging) dedicated to  $\text{CO}_2$  measurements<sup>34</sup>. Finally, transition frequencies measured at the kHz level  
82 can also be used to increase the accuracy of several other transition frequencies through the  
83 application of the Ritz principle or effective Hamiltonian models<sup>35</sup>.

84 Regarding the experiment, in order to circumvent the Doppler line broadening, the  
85 measurements were performed by CRDS in saturation regime<sup>36</sup>. The CRDS technique is well-adapted  
86 for Lamb-dip frequency measurements thanks to the narrow (kHz level) resonances of the high-  
87 finesse optical cavities and the high intracavity power<sup>37,38</sup>. After a description of the experimental  
88 set-up and recorded transitions (Part 2), we will detail the data analysis and error budget (Part 3).  
89 The spectroscopic constants of the two bands studied will be derived from a fit of the measured  
90 upper energy levels and the final set of recommended position values will be compared to available  
91 literature data in Part 4, before the concluding remarks (Part 5).

92

## 93 **2. Experimental set-up and recorded transitions**

94 Measurements were performed with an improved version of the comb-referenced cavity ring  
95 down spectrometer described in Mondelain *et al.*<sup>32</sup> and shown in **Fig. 2**. This spectrometer is based  
96 on an extended cavity diode laser (ECDL) (New Focus; Model TLB 6736) covering the 1975-2075 nm  
97 range. A large part (90%) of the emitted laser power is coupled to a temperature regulated high  
98 finesse cavity (HFC) described in Vasilchenko *et al.*<sup>39</sup> via an acousto-optic modulator (AOM) (to  
99 produce the ring down (RD) events) and an electro-optic modulator (EOM) to correct from laser jitter  
100 and phase noise (DC to >40 MHz correction bandwidth) as explained below. The 45 cm-long high  
101 finesse cavity is made of two high reflectivity mirrors (from Layertec, with a reflection coefficient  
102  $R > 99.99\%$  over the 1950-2250 nm range). Periodic resonances between the laser light and the cavity

103 modes are achieved by applying a voltage triangular ramp on the PZT tube on which the output  
 104 cavity mirror is mounted. At resonance, the AOM (model ACM-1002AA1 from IntraAction Corp.) is  
 105 used to switch off the injection of photons in the cavity and generate a RD event detected by an  
 106 extended InGaAs PIN photodiode (G12183 series from Hamamatsu). Typical RD times of the  
 107 evacuated cell are  $\tau = 55 \mu\text{s}$  at  $4875 \text{ cm}^{-1}$  and  $48 \mu\text{s}$  at  $4953 \text{ cm}^{-1}$ .

108 In our previous works<sup>4,32,39</sup>, a beat note (BN) signal, between the laser source and the closest  
 109 tooth of a frequency comb (FC), was used to accurately determine the absolute frequency of the  
 110 laser source, limited by a laser line width of a few hundred kHz. Here, this signal is used to transfer  
 111 the coherence of the comb to a fraction of the ECDL output using the feed-forward technique,  
 112 described in Votava *et al.*<sup>40</sup> and in Gotti *et al.*<sup>41</sup>, providing a driftless and spectrally narrower source  
 113 directly tunable using a RF synthesizer. In more detail, the BN signal is first low-pass filtered (BLP-  
 114 150+ from Mini-Circuits; 150 MHz cut-off) to select only the BN with the closest comb tooth,  
 115 amplified with a series of three amplifiers (ZFL500LN+ from Mini-Circuits; 28 dB of gain), and then  
 116 separated with a power splitter (PSC-2-1 from Mini-Circuits; 0.1 to 400 MHz). The first output  
 117 channel is digitized by a fast acquisition card (250 MHz-16 bits, by GAGE) which gives the BN  
 118 frequency,  $f_{BN}$ , after Fourier transform of this signal and a peak determination procedure over the 0  
 119 to 125 MHz RF range at a 350 Hz repetition rate with a 15 kHz resolution. The BN linewidth is a  
 120 combination of comb tooth and ECDL linewidths (which dominates) and is typically **200 kHz** FWHM.  
 121 This BN frequency measurement, previously used for frequency calibration, is only used here to  
 122 stabilize the ECDL frequency around  $f_{BN} = 55 \text{ MHz}$  via the *Current modulation* input of the controller.  
 123 The second output channel is mixed with a signal from a RF synthesizer (SMA100B from  
 124 Rohde&Schwarz ; 8 kHz - 20 GHz) in a single-side band modulator (TRF370417 50-MHz to 6-GHz  
 125 Quadrature Modulator from Texas Instruments), then amplified to feed the RF input of the EOM  
 126 (MPZ-LN-10 from iXBlue ; electro-optical bandwidth > 10 GHz; central wavelength: 1550 nm). This  
 127 latter generates a corrected and an uncorrected side band in addition to the carrier frequency with  
 128 the following frequencies:

$$129 \quad \nu_{carrier} = n f_{rep} + f_{CEO} + \text{sign} f_{BN} \quad (1)$$

$$130 \quad \nu_{side\ band\_nc} = n f_{rep} + f_{CEO} + \text{sign} f_{BN} - \text{sign}(f_{synth} - f_{BN}) \quad (2)$$

$$131 \quad \nu_{side\ band\_c} = n f_{rep} + f_{CEO} + \text{sign} f_{BN} + \text{sign}(f_{synth} - f_{BN}) \quad (3)$$

132 where  $f_{rep} = 250 \text{ MHz}$  and  $f_{CEO} = -20 \text{ MHz}$  are the repetition rate and the carrier-envelope offset of the  
 133 FC referenced to a 10 MHz rubidium frequency standard (Model PRS 10 from SRS) (hereafter called  
 134 *RF lock*) which is phase-locked to a GPS timing receiver.  $n$  is the comb tooth number determined with  
 135 a commercial wavelength meter (HighFinesse WS7-60 IR-II). *Sign* is equal to + or - and corresponds  
 136 to the sign of the BN.  $f_{synth}$  is the frequency generated by the RF synthesizer to add a programmable

137 shift to  $f_{BN}$  (which is kept close to 55 MHz). Note that, as indicated in **Table 1** and **Table 2** part of the  
138 measurements were performed with the comb *optically* locked *via* an intra-cavity EOM to an ultra-  
139 stable optical frequency (known with accuracy at the  $10^{-16}$  level) at 1542 nm (~194 417 936 MHz)  
140 (hereafter called *Optical* lock). This frequency standard is transferred to our laboratory from the LNE-  
141 SYRTE in Paris over about 1000 km through a dedicated line of the RENATER academic fiber network  
142 thanks to the French Equipex project REFIMEVE+<sup>42</sup>.

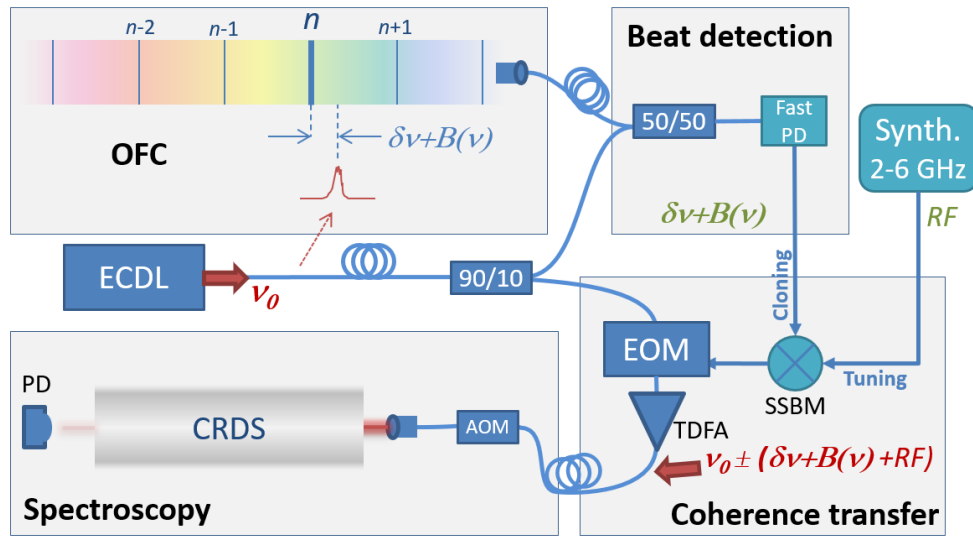
143 As can be seen from Eq. (3), the BN frequency is eliminated for the corrected sideband frequency.  
144 This means that the jitter and also higher frequency phase noise of the laser source (*i.e.* the ECDL) is  
145 suppressed for this sideband making it a frequency-shifted clone of a comb tooth, with the  
146 programmable offset given by  $f_{synth}$ . This clone possess the comb tooth linewidth which is typically  
147 100 kHz and **5 kHz** for the *RF* and *Optical* locks, respectively instead of a few hundred kHz (at a 1 ms  
148 time scale) for the ECDL emission width. On the other hand, Eq. (2) shows that for the uncorrected  
149 frequency we have two times the BN frequency, leading to a broadening of this side band relative to  
150 the carrier.

151 The output of the EOM is then amplified by a cw –Thulium -doped fiber amplifier (CTFA-PB-PM-  
152 20-BW4 from Keopsys; central wavelength: 2004 nm; saturated output power: 17 to 40 dBm) before  
153 passing through the AOM and the high finesse cavity. The RF signal (94.15 MHz) applied to the AOM  
154 is generated by a direct digital synthesizer (DDS) referenced to the 10 MHz rubidium frequency  
155 standard as well as the RF synthesizer. Note that the laser frequency in the cavity has to be corrected  
156 from the AOM frequency used here in its order -1. The feed-forward "correction" is optimized by  
157 placing an optical delay line (*i.e.* a 5 m long optical fiber) before the EOM.

158 Note that in the previous works<sup>40,41</sup> a telecom dual Mach-Zehnder modulator (MZM) was used.  
159 Unfortunately, this optical component is not available in the 2  $\mu\text{m}$  spectral range, leading us to use  
160 an EOM. This latter has the drawback of having both side bands and the carrier sent in the HFC  
161 instead of only one side band for the MZM (the carrier and the other side band being suppressed in  
162 this case). This leads to potential frequency crossing between the corrected side band and the carrier  
163 and other side bands, since the latter become resonant with the HFC if they are separated by a  
164 multiple of the free spectral range, complicating the (large) tuning. Note that even if the operating  
165 wavelength of the EOM is 1.55  $\mu\text{m}$ , it works in the 2  $\mu\text{m}$  region only with small additional losses  
166 which illustrates the large spectral coverage of this optical component. Unfortunately, integrated  
167 MZM devices do not appear to be so versatile.

168 Spectra are acquired step by step by changing  $f_{synth}$  which can be tuned in our setup between 2  
169 and 6 GHz (due to technical limitation of our RF electronics). In the case of Lamb dip acquisitions,  
170 each spectrum corresponds to a scan over 4 MHz with spectral steps of 20 kHz. At each spectral step,  
171 150 or 200 RD events are averaged. The scan duration is about 5 min.

172



173

174

175

176

177

178

**Fig. 2.** Scheme of the experimental set-up. OFC: Optical frequency comb, AOM: acousto-optic modulator, EOM: electro-optic modulator, ECDL: external cavity diode laser, SSBM: single side band modulator, TDF: Thulium doped fiber amplifier, PD: photo-diode.  $B(\nu)$  and  $\delta(\nu)$  represent the beat note frequency and its noise, respectively.

179

180

181

182

183

184

The HFC is filled by a flow of pure  $\text{CO}_2$  (from Air Liquide; 99.995% of purity). The pressure inside the cell is measured thanks to a MKS Baratron 626B absolute pressure transducer (1.33 mbar full scale; 0.25% uncertainty of reading) and controlled with an electro-valve (2871 series from Burkert; 0.3 mm orifice dia.) and homemade PID software. The temperature of the sounded gas is measured with an accuracy of 0.04 K and the temperature homogeneity of the gas in the HFC is better than 0.05 K (see Vasilchenko *et al.* <sup>39</sup> for the details).

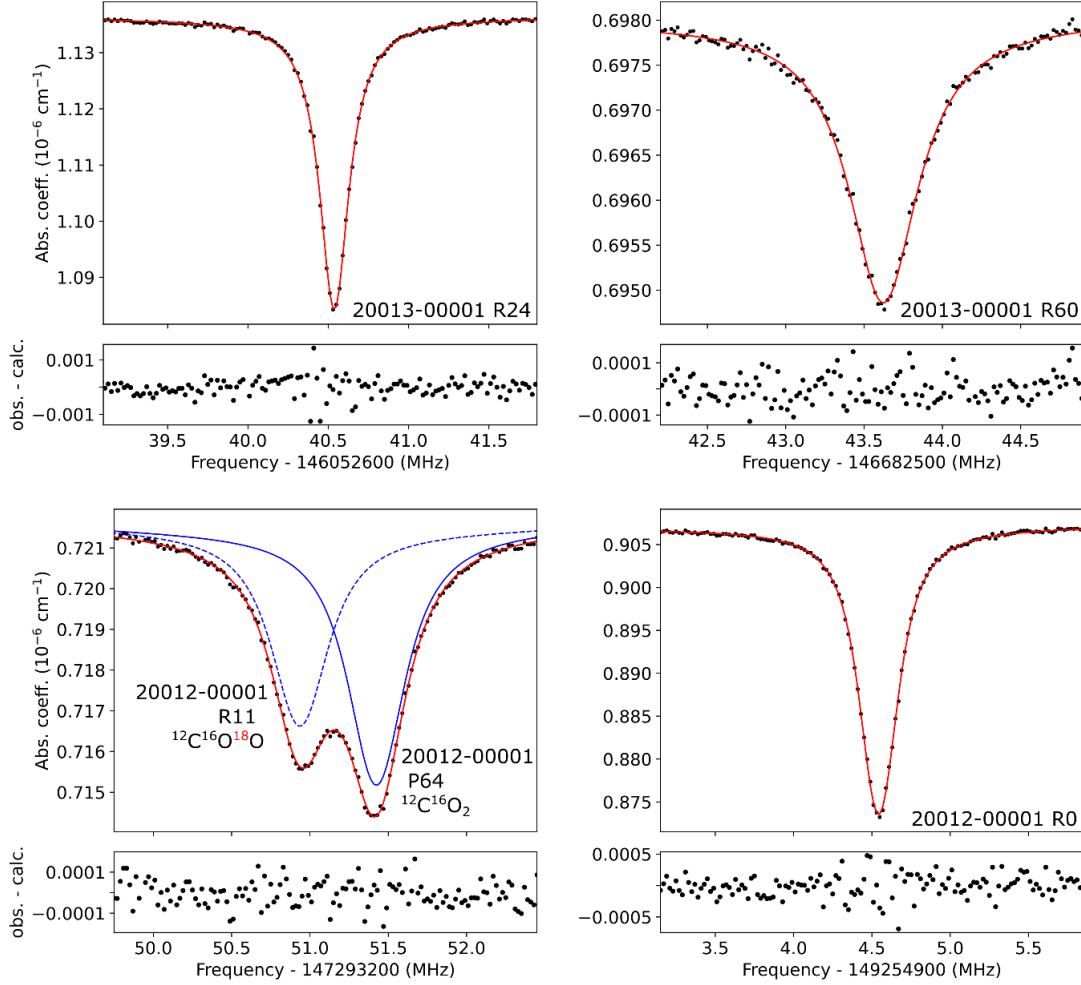
185

186

187

In this work, 63 transitions up to  $J''= 74$  and 43 transitions up to  $J''= 70$  have been studied from Lamb dip spectra for the 20012-00001 and 20013-00001 band, respectively. The measured transitions are highlighted in **Fig. 1**. Several examples of Lamb dips spectra are presented in **Fig. 3**.





188

189 **Fig. 3.** Examples of Lamb dips (dotted points) for the R(24) (upper left panel) and R(60) (upper right panel)  
 190 transitions of the 20013-00001 band of  $^{12}\text{CO}_2$ , and the P(64) (lower left panel) and R(0) (lower right panel)  
 191 transitions of the 20012-00001 band of  $^{12}\text{CO}_2$ . The frequency step is 20 kHz and the indicative pressure values  
 192  $P_{\text{CO}_2}$  are about 0.04, 13, 7 and 0.03 Pa, respectively. Note that for the P(64) transition, an additional Lamb dip is  
 193 visible, due to the R(11) transition of the 20012-00001 band for the  $^{12}\text{C}^{16}\text{O}^{18}\text{O}$  isotopologue. The fits using a  
 194 Voigt profile (red solid line) are also shown on the figure as well as the residuals (obs. – calc.) plotted on the  
 195 small panels below each graph.

196

### 3. Data analysis and error budget

197

#### A. Data analysis

198

199

200

201

202

203

204

As already reported<sup>37,40,43,44</sup> in the case of a saturated line profile, the ring down signals are no  
 more a purely decreasing exponential with time. In Giusfredi *et al.*<sup>37</sup>, a non-exponential model was  
 proposed to fit the ring down events and to obtain more reliable Lamb dip profiles. However, in the  
 studies dedicated to transition frequency retrievals from Lamb dips, a simple exponential treatment  
 is generally adopted<sup>10,12,38,45</sup> arguing that this should not bias the determination of the center  
 frequency of the absorption line due to the symmetry of the saturation spectrum.

205 The four examples of Lamb dips displayed on **Fig. 3** result from the RD fit with a purely  
 206 exponential function. The Lamb dip profiles are then fitted with a Voigt function for which the  
 207 Lorentzian widths as well as the dip amplitude and a second order polynomial baseline are free to  
 208 float. This results in residuals at the noise level (lower panels of **Fig. 3**). Typical fitted values of  
 209 Lorentzian widths are between 130 and 250 kHz (FWHM). Interestingly, no Gaussian contribution  
 210 was necessary for the Lamb dips recorded for the 20013-00001 band while for the 20012-00001  
 211 band, a Gaussian contribution with a typical width of 110 kHz (FWHM) had to be added. **Fig. 3**  
 212 illustrates the very good quality factor (QF defined as the ratio of the change of absorption of the dip  
 213 to the *rms* of the residuals) that can be achieved with a value close to 200 for the R(0) transition, as  
 214 well as the pressure broadening which was observed for the higher *J* transitions such as R(60) for  
 215 which a larger pressure value was used. The lower left panel shows an interesting feature with two  
 216 Lamb dips accidentally close to each other, one corresponding to the P(64) transition of the 20012-  
 217 00001 band of  $^{12}\text{CO}_2$ , as expected, and the second one to the R(11) transition for the same band but  
 218 for the  $^{12}\text{C}^{16}\text{O}^{18}\text{O}$  isotopologue (the assignment of the P(64) 20012-00001 dip of  $^{12}\text{CO}_2$  was  
 219 established using combination difference relation – see below). The frequency of the R(11) transition  
 220 of the  $^{12}\text{C}^{16}\text{O}^{18}\text{O}$  isotopologue is also reported in the Supplementary Material, as well as for the P(12)  
 221 transition.

222 For each transition, 10 spectra are generally recorded showing a statistical dispersion on the line  
 223 centers below 2 kHz for all the transitions with  $J'' \leq 70$  for the 20012-00001 band and  $J'' \leq 62$  for the  
 224 20013-00001 band. **Table 1** and **Table 2** list the studied transitions with their measured frequencies,  
 225 estimated final uncertainties and the number of recorded spectra for each of them, as well as the  
 226 indicative pressure value.

227

Assig.	Freq. (kHz)	Pres. (Pa)	# of spectra	Lock	Final unc. (kHz)
P16	145119049920.6	0.13	3	RF	3.0
P14	145169371981.4	0.13	6	RF	3.4
P12	145219201993.0	0.13	9	RF	3.5
P10	145268542644.7	0.07	8	RF	3.4
P8	145317396075.5	0.07	7	RF	3.6
P6	145365763879.6	0.14	9	RF	3.2
P4	145413647096.5	0.03	10	Opt.	3.1
P2	145461046214.5	1.20	9	RF	3.4
R0	145531236890.1	2.00	21	RF	3.4
R2	145577424223.3	0.73	6	RF	3.1
R4	145623124768.3	0.03	10	Opt.	2.9
R6	145668336501.3	0.03	10	Opt.	3.0
R8	145713056851.0	0.03	9	Opt.	2.9
R10	145757282685.6	0.03	6	Opt.	3.4
R12	145801010333.2	0.03	10	Opt.	3.0

R14	145844235571.7	0.03	10	Opt.	2.9
R16	145886953640.9	0.03	10	Opt.	2.9
R18	145929159249.7	0.03	10	Opt.	3.0
R20	145970846578.6	0.03	10	Opt.	2.9
R22	146012009289.8	0.03	11	Opt.	2.9
R24	146052640536.8	0.04	10	Opt.	2.9
R26	146092732967.0	0.07	10	Opt.	3.1
R28	146132278738.5	0.07	10	Opt.	3.0
R30	146171269531.1	0.12	30	Opt.	3.3
R32	146209696545.2	0.12	20	Opt.	3.1
R34	146247550532.3	0.12	20	Opt.	3.0
R36	146284821792.1	0.16	168	Opt.	2.9
R38	146321500193.2	0.18	21	Opt.	3.0
R40	146357575182.8	0.19	16	Opt.	2.9
R42	146393035800.0	0.20	10	Opt.	3.0
R44	146427870697.5	0.16	10	Opt.	3.0
R46	146462068137.7	0.16	10	Opt.	2.9
R48	146495616036.8	0.16	10	Opt.	3.0
R50	146528501949.4	1.41	20	Opt.&RF	3.2
R52	146560713096.8	2.67	6	RF	3.3
R54	146592236384.6	2.67	9	RF	3.5
R56	146623058410.3	2.67	9	RF	3.2
R58	146653165481.7	6.67	9	RF	3.8
R60	146682543621.6	13.33	9	RF	3.4
R62	146711178600.3	13.33	10	RF	3.4
R64	146739055925.1	20	10	RF	7.7
R66	146766160861.4	16.29	18	RF	6.5
R68	146792478469.7	26.66	10	RF	14.6

228 **Table 1.** Frequencies of the transitions of the 20013-00001 band of  $^{12}\text{CO}_2$  determined in this work with their  
229 final uncertainties (see text and **Table 3**). The frequencies are given after correction of the 90 Hz second-order  
230 Doppler shift. RF and Opt correspond to the RF lock and optical lock (see text for details), respectively.  
231

Assig.	Freq. (kHz)	Pres. (Pa)	# of spectra	Lock	Final unc. (kHz)
P74	146911623361.5	20	10	RF	8.7
P72	146989515840.3	13.33	10	RF	4.0
P70	147066640733.3	13.33	10	RF	3.5
P68	147142980565.8	6.67	10	RF	3.5
P66	147218521294.3	6.67	18	RF	3.4
P64	147293251422.9	6.67	12	RF	3.7
P62	147367161400.9	6.67	9	RF	3.3
P60	147440243211.6	6.67	10	RF	3.3
P58	147512490048.1	6.67	10	RF	3.3
P56	147583896096.4	6.67	10	RF	3.3
P54	147654456358.4	6.66	10	RF	3.3
P52	147724166519.3	0.07	10	RF	3.0
P50	147793022842.6	0.03	10	RF	3.1
P48	147861022080.7	0.03	10	RF	3.0
P46	147928161407.1	0.03	10	RF	3.1
P44	147994438380.1	0.03	10	Opt.	3.3

P42	148059850796.9	0.03	10	Opt.	3.0
P40	148124396819.3	0.03	10	Opt.	2.9
P38	148188074787.2	0.03	10	Opt.	2.9
P36	148250883255.1	0.03	9	Opt.	2.8
P34	148312820947.2	0.03	10	Opt.	2.9
P32	148373886735.5	0.03	10	Opt.	2.9
P30	148434079613.5	0.03	10	Opt.	2.9
P28	148493398682.7	0.03	10	Opt.	3.9
P26	148551843131.1	0.03	10	Opt.	2.9
P24	148609412204.0	0.03	10	Opt.	3.0
P22	148666105210.8	0.02	13	RF	3.1
P20	148721921498.3	0.02	10	RF	3.0
P18	148776860436.3	0.02	10	RF	3.0
P16	148830921417.8	0.02	10	RF	3.0
P14	148884103839.8	0.02	10	RF	3.2
P12	148936407097.7	0.02	3	RF	3.1
P10	148987830579.6	0.02	20	RF	3.6
P8	149038373657.5	0.03	14	Opt.	2.9
P6	149088035683.0	0.03	10	Opt.	2.9
P4	149136815987.3	0.03	7	Opt.	2.9
P2	149184713867.3	0.03	10	Opt.	3.0
R0	149254904543.6	0.03	10	Opt.	3.1
R2	149300593110.5	0.03	8	Opt.	2.9
R4	149345396570.0	0.03	10	Opt.	2.9
R6	149389314083.5	0.03	10	Opt.	2.9
R8	149432344784.5	0.02	20	RF	3.1
R10	149474487792.4	0.02	5	RF	3.1
R12	149515742194.7	0.02	10	RF	3.0
R14	149556107069.8	0.01	16	RF	3.2
R16	149595581482.8	0.01	9	RF	3.1
R18	149634164511.2	0.01	6	RF	3.0
R20	149671855220.4	0.01	10	RF	3.1
R22	149708652707.4	0.01	5	RF	2.9
R24	149744556091.7	0.01	9	RF	3.1
R26	149779564532.6	0.01	9	RF	3.2
R28	149813677243.6	0.01	10	RF	3.1
R30	149846893508.5	0.01	10	RF	3.1
R32	149879212692.8	0.01	10	RF	3.0
R34	149910634270.4	0.01	10	RF	3.0
R36	149941157834.1	0.01	9	RF	3.3
R38	149970783128.6	0.01	10	RF	3.1
R40	149999510067.7	0.01	9	RF	3.2
R42	150027338777.9	0.01	10	RF	3.2
R44	150054269570.1	0.01	9	RF	3.2
R46	150080303113.5	0.01	10	RF	3.3
R48	150105440317.6	0.01	10	RF	3.1
R50	150129682483.6	0.01	9	RF	3.2

233

**Table 2.** Same as **Table 1** for the 20012-00001 band of  $^{12}\text{CO}_2$ .

234

235

**B. Error budget**

236

The different sources of uncertainties on the zero-pressure line frequencies reported in **Table 1**

237

and **Table 2** are discussed below and summarized in **Table 3**.

238

239

240

**Table 3.** Uncertainty budget of the low pressure transition frequencies reported in **Table 1** for the 20013-00001 band and in **Table 2** for the 20012-00001 band. The *Freq. shift* column corresponds to the correction applied to the measured frequencies.

Source of uncertainty	Freq. shift (kHz)	Uncertainty (kHz)
<b>Statistics</b>		<2.0 <sup>a</sup>
<b>RF comb lock</b>		0.73
<b>Optical comb lock</b>		<0.001
<b>1<sup>st</sup> order Doppler shift</b>		0.6
<b>2<sup>nd</sup> order Doppler shift</b>	0.09	<0.001
<b>AC and DC Stark shift</b>		<0.01
<b>Power shift</b>		2
<b>Pressure shift</b>		<1 <sup>b</sup>
<b>RD treatment</b>		2
<b>Total</b>	<b>0.09</b>	<b>&lt;4<sup>b</sup></b>

241

Notes:

242

<sup>a</sup> For all the transitions with  $J \leq 70$  for the 20012-00001 band and  $J \leq 62$  for the 20013-00001 band.

243

<sup>b</sup> For 102 over 107 transitions.

244

245

According to Eq. (3), the frequency of the laser light injected in the cavity only depends on  $f_{\text{rep}}$ ,

246

$f_{\text{CEO}}$ ,  $f_{\text{synth}}$  and  $f_{\text{AOM}}$ . All these frequencies are referenced to a 10 MHz Rb frequency standard (Model

247

PRS 10 from SRS) which is phase-locked to a GPS timing receiver leading to a (short-term and long-

248

term) stability  $< 5 \times 10^{-12}$ . This leads to negligible uncertainties on the four frequencies but as  $f_{\text{rep}}$  has to

249

be multiplied by the tooth number (between  $\sim 581\,200$  and  $587\,700$  in our studied range) when the

250

comb is *RF* locked, it leads to uncertainties between 726 and 734 Hz. Note that for the *optical* lock

251

the reference frequency is known with an accuracy at the  $10^{-16}$  level, reducing drastically the

252

uncertainty on the corrected side-band frequency. To check the impact of the *RF* and *optical* locks,

253

we recorded 36 spectra of the P(12) transition in the 20012-00001 band with the comb *optically*-

254

locked followed by 46 spectra with the comb *RF*-locked. We observe a decrease of 760 Hz of the

255

mean frequency value in the *RF*-lock case compared to the *Optical*-lock case (with standard error of

256

the mean of 138 and 130 Hz, respectively). This difference is close to the estimated uncertainty of

257

the *RF*-lock. Additionally, the QF of the Lamb dip is improved with the optical lock from 175 to 253 in

258

average.

259

The possible impact of the pressure shift on the Lamb dip center values has to be considered as it

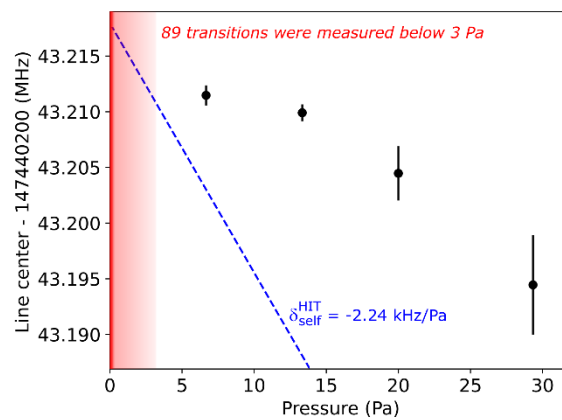
260

might affect the frequency at zero-pressure. For this purpose, we measured several Lamb dip spectra

261

for the weak P(60) transition in the 20012-00001 band at pressure values of about 7, 13, 20 and  $\sim 30$

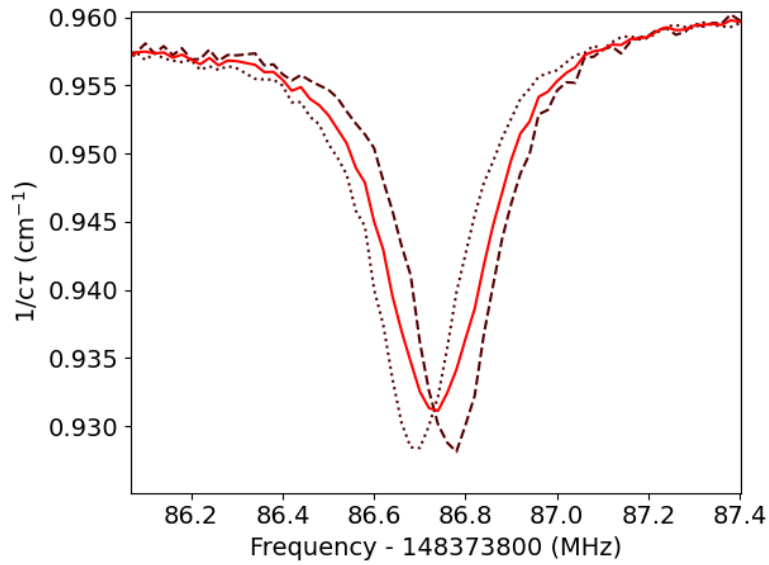
262 Pa (Note that most of our measurements rely on spectra recorded at much lower pressure, below 1  
 263 Pa – see **Table 1** and **Table 2**). The pressure dependence of the Lamb dip centers averaged over all  
 264 the spectra at a given pressure are plotted on **Fig. 4**. As expected from Fig 2 (case *a*) of Alekseev *et*  
 265 *al.*<sup>46</sup> and from Fig. 2 of Bagaev *et al.*<sup>47</sup> (or identically Fig. 4.35 of Letokhov<sup>48</sup>), a non-linear dependence  
 266 of the pressure-shift with the pressure is observed. This is due to the transition from the low  
 267 pressure regime towards the usual high pressure collisional regime. As a result, the pressure-shift is  
 268 observed to evolve from a value of  $\sim -0.23$  kHz/Pa (or  $-7.8 \times 10^{-4}$  cm<sup>-1</sup> atm<sup>-1</sup>) at very low pressure to an  
 269 high pressure value which has a 10 times larger amplitude ( $-2.24$  kHz/Pa or  $-7.57 \times 10^{-3}$  cm<sup>-1</sup>/atm)  
 270 according to HITRAN2020<sup>49</sup>. This variation is similar to that reported in Tan *et al.*<sup>14</sup> for the P(10)  
 271 transition of the 30012-00001 band of <sup>12</sup>CO<sub>2</sub>: a pressure shift of  $-0.35 \pm 0.08$  kHz/Pa was measured  
 272 below 4 Pa, *i.e.* a four times smaller amplitude than the  $-1.7$  kHz/Pa pressure-shift coefficient  
 273 recommended in the HITRAN database. The uncertainty due to the pressure shift was estimated by  
 274 fitting a second order polynomial function to the data points of **Fig. 4**. Thanks to the very low  
 275 pressures adopted for most of the Lamb dip measurements (**Table 1** and **Table 2**), the pressure-shift  
 276 has a negligible contribution ( $< 1$  kHz) for most of the transitions. Note that if the usual pressure-shift  
 277 values are used to get zero-pressure frequencies from measurements in the low pressure *regime*<sup>8,12</sup>,  
 278 errors could be introduced.



279  
 280 **Fig. 4.** Pressure dependence of the Lamb dip center for the P(60) transition of the 20012-00001 band of  
 281 <sup>12</sup>CO<sub>2</sub>. The dashed blue line represents the self-pressure shift coefficient reported in HITRAN2020 for the same  
 282 transition.

283  
 284 Another source of uncertainty in our experimental set-up could be due to the Doppler frequency  
 285 shift, induced by the moving speed of the output mirror mounted on the piezo-actuator and  
 286 accumulated during the recorded light decays. To quantify this possible bias we have slightly  
 287 modified the acquisition software and the set-up to distinguish between the RD events obtained for  
 288 the increasing part of the triangular voltage function applied to the piezo actuator (RD<sub>i</sub>) and those

289 obtained for the decreasing part (RD<sub>d</sub>).). As shown on **Fig. 5**, a shift between the Lamb dips retrieved  
 290 from RD<sub>i</sub> and RD<sub>d</sub> is clearly visible. For the triangular function parameters applied during all the  
 291 measurements, the observed shift is typically equal to 80 kHz. A bias could occur if the number of  
 292 RD<sub>i</sub> and RD<sub>d</sub> differs. From several Lamb dip spectra, differences of a few percent can be observed  
 293 between the number of RD<sub>i</sub> and RD<sub>d</sub>. This leads to a small bias between the “true” frequency  
 294 corresponding to the mean of the two Lamb dip frequencies and the one retrieved when all RDs are  
 295 considered. From these measurements, an estimated uncertainty of 0.6 kHz due to this 1<sup>st</sup> order  
 296 Doppler shift effect is adopted in the budget error.



297  
 298 **Fig. 5.** Example of Lamb dips for the P(32) transition of the 20012-00001 band. The Lamb dips are obtained from  
 299 the RDs corresponding to the increasing (dashed line) and decreasing (dotted line) part of the triangular voltage  
 300 function applied to the piezo actuator on which the output mirror is mounted. Note the shift of 77 kHz between  
 301 the two Lamb dips due to the 1<sup>st</sup> order Doppler effect. The red solid line corresponds to the Lamb dip retrieved  
 302 from all the RD events.

303  
 304 Measured absolute frequencies have to be corrected from the 2<sup>nd</sup> order Doppler shift by  
 305  $\nu_0 = \nu_{meas} + \frac{\nu_0}{c^2} \frac{k_B T}{m}$  <sup>36</sup> with  $c$  the speed of light in vacuum,  $k_B$  the Boltzmann constant,  $T$  the gas  
 306 temperature in K and  $m$  the molecular mass of <sup>12</sup>C<sup>16</sup>O<sub>2</sub> mass. The correction that we applied to the  
 307 measured frequencies is between 90.5 and 93.5 Hz depending on the transition with an uncertainty  
 308 of ~15 mHz due to the gas temperature uncertainty.

309 The AC Stark shift due to the intracavity optical field, as well as the DC Stark shift which could be  
 310 due to the static charge buildup on the cavity mirrors, have to be considered<sup>12,43</sup>. Based on the  
 311 isotropic,  $\tilde{\alpha}$ , and anisotropic,  $\Delta\tilde{\alpha}$ , polarizabilities of the CO<sub>2</sub> molecule in its ground state and excited  
 312 vibrational states<sup>50</sup>, we obtain the DC Stark shift from Eq. 1 of Cai *et al.*<sup>51</sup> and the AC Stark shift from

313  $\delta\nu_{AC Stark} = -\frac{1}{4}\delta\tilde{\alpha}E^2$ <sup>52</sup>. The calculated impact on the measured frequencies is at the Hz level  
 314 (taking a static field strength of 30 kV/m as in Reed *et al.*<sup>12</sup> and an intracavity optical field strength of  
 315 19.6 kV/m), so completely negligible.

316 In addition, we investigated experimentally the potential shift due to intra-cavity power by  
 317 recording series of Lamb dip spectra for the P(40) transition of the 20012-00001 band with four levels  
 318 of RD threshold corresponding to different intra-cavity power at the RD starting point (between 0.15  
 319 and 0.45 W). A maximum variation of ~2 kHz is observed between the four data points. This value is  
 320 consistent with what is obtained by adopting different thresholds in the analysis of the RDs. An  
 321 uncertainty of 2 kHz due to the power shift is thus integrated in the budget error for all the  
 322 transitions.

323 As a test of our modeling of the RD signal with a standard exponential function, we considered a  
 324 treatment using a non-linear exponential function in order to take into account the fact that, in the  
 325 saturation regime, the absorption coefficient depends on the light intensity in the form<sup>37</sup>:

$$326 \quad \alpha(I) = \alpha_{cav} + \alpha_{gas} \frac{1}{\sqrt{1+I/I_S^*}} \quad (4)$$

327 where  $\alpha_{cav}$  is the empty-cavity loss,  $\alpha_{gas}$  is the unsaturated molecular absorption and  $I_S^*$  is the  
 328 saturation intensity. The non-linear exponential function was calculated in a recursive manner and  
 329 led to residuals of the RD fit at the noise level. Due to correlations, the obtained parameters were  
 330 very noisy if floated all together. Fixing  $\alpha_{cav}$  which can reasonably be expected to be constant over  
 331 the range of a given spectrum, has led to frequency shifts on the order of 2 kHz when fitting the  
 332 obtained  $I_S^*$  as compared to the frequency values reported here using a purely exponential fit. The  
 333 origin of these shifts needs further investigations. An additional uncertainty of 2 kHz was thus added  
 334 for all the transitions to take into account the impact of the ring-down treatment.

335

#### 336 **4. Spectroscopic analysis and comparison to literature**

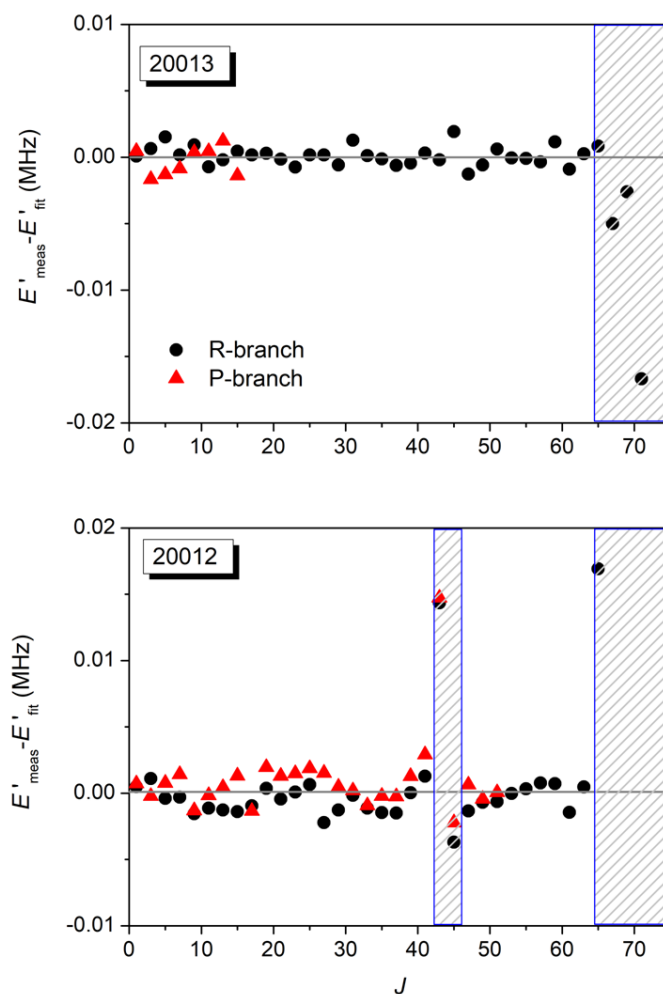
337 For an isolated vibrational state, the energy values of the rotational levels can be reproduced with  
 338 the standard expression:

$$339 \quad E(J) = G_v + B_v J(J+1) - D_v J^2(J+1)^2 + H_v J^3(J+1)^3 + L_v J^4(J+1)^4 + M_v J^5(J+1)^5 + \\ 340 \quad N_v J^6(J+1)^6 + O_v J^7(J+1)^7 + \dots \quad (5)$$

341 where  $G_v$  is the vibrational term and  $B_v \dots O_v$  are the rotational and centrifugal distortion constants.  
 342 The experimental value of the energy of the upper rotational levels in the 20012 and 20013  
 343 vibrational states was obtained by adding the lower state energy values to the measured transition  
 344 frequencies. The <sup>12</sup>CO<sub>2</sub> ground state rotational constants determined in Wu *et al.*<sup>10</sup> with a very high  
 345 accuracy were used to calculate the ground state energy levels. The spectroscopic constants of the  
 346 20012 and 20013 upper states were derived from a fit of the obtained upper state energy values.



347 (Note that each energy level has generally two experimental determinations from the  $R(J-1)$  and  
 348  $P(J+1)$  transitions). Applying Eq. (5) of Wu *et al.*<sup>10</sup> to the transitions measured in this work for the  
 349 20012-00001 and 20013-00001 bands and fixing the  $B''$ ,  $D''$ ,  $H''$  and  $L''$  constants to the values  
 350 reported in the Table 2 of Wu *et al.*<sup>10</sup>, we are able to reproduce our experimental ground  
 351 combination differences at the kHz level (mean difference of 1.0 kHz;  $1\sigma$ -standard deviation of 1.2  
 352 kHz), confirming the work of Wu *et al.*<sup>10</sup> up to  $J=63$ . Energy levels up to  $J\leq 63$  were thus included in  
 353 our fit. The fitted spectroscopic constants listed in **Table 4** allow reproducing the energy levels of the  
 354 20012 and 20013 states with a (meas.- calc.) standard deviation of 1.1 kHz and 0.8 kHz, respectively.



355  
 356 **Fig. 6.** Difference between the measured rotational energy levels,  $E'_{\text{meas}}$  and the values fitted using Eq. (5),  
 357  $E'_{\text{fit}}$ , for the 20013 and 20012 vibrational states (upper and lower panel, respectively). Red triangles and black  
 358 dots correspond to energy levels obtained from P- and R-transitions, respectively. The dashed zones correspond  
 359 to J values excluded from the fit.  
 360

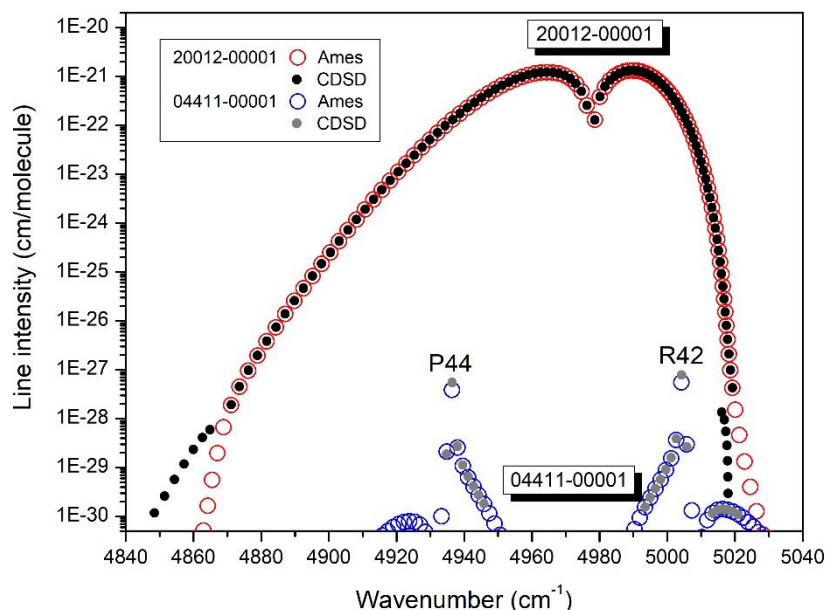
361  
362  
363  
364  
365

**Table 4.** Ro-vibrational constants (in MHz) of the 20012 and 20013 vibrational states of  $^{12}\text{CO}_2$ . The fit was limited to  $J \leq 63$  excluding the perturbed  $J= 43$  and 45 energy levels of the 20012 state (see text).  $N_{fit}$  and  $N_{meas}$  represent the number of levels included in the fit and measured, respectively.

Parameter (MHz)	20012	20013
<i>G</i>	$1.492317285961(5) \times 10^8$	$1.455079611574(3) \times 10^8$
<i>B</i>	$1.1587981508(6) \times 10^4$	$1.1637877181(4) \times 10^4$
<i>D</i>	$4.08036(2) \times 10^{-3}$	$5.45134(1) \times 10^{-3}$
<i>H</i>	$2.187(3) \times 10^{-8}$	$1.818(1) \times 10^{-8}$
<i>L</i>	$1.4(2) \times 10^{-13}$	$-3.2(5) \times 10^{-14}$
<i>M</i>	$1.38(9) \times 10^{-16}$	$-2.5(1) \times 10^{-17}$
<i>N</i>	$-2.1(2) \times 10^{-20}$	$9.8(10) \times 10^{-22}$
<i>O</i>	$3.1(1) \times 10^{-24}$	
$N_{fit}/N_{meas}$	54/63	40/43
<i>rms</i> (Hz)	1100	808

366 The residuals of the fit plotted in **Fig. 6** indicate that the  $J= 43$  and 45 rotational energy levels of  
367 the 20012 state (excluded from the fit) are affected by a local resonance interaction around  $J= 43$ .  
368 The very small energy perturbation on the order of 15 kHz at  $J= 43$  is confirmed by the very close  
369 value of the residuals obtained from the P(44) and R(42) Lamb dip centers. By consideration of the  
370 theoretical calculations of the  $^{12}\text{CO}_2$  spectrum by the Ames group<sup>53</sup> and in the Carbon Dioxide  
371 Spectroscopic Databank (CDSDB)<sup>35</sup>, the perturber state could be identified as the 04411 vibrational  
372 state. Both calculations predict that the rotational levels of the 20012 and 04411 exhibit an energy  
373 crossing with an energy separation of only  $0.15 \text{ cm}^{-1}$  at  $J= 43$ . The 20012  $J= 43$  energy level being  
374 larger than its 04411 counterpart, the perturbation leads to a shift to higher energy of the 20012  $J=$   
375 43 level, in agreement with experiment. Note that the energy separation between the next  $J= 45$   
376 level is predicted to be significantly larger ( $0.47 \text{ cm}^{-1}$ ) and of opposite sign, in agreement with the  
377 observation of a more reduced and negative shift of the 20012  $J= 43$  level from its unperturbed  
378 position (about -3 kHz). We present in **Fig. 7**, the spectrum of the 20012-00001 and 04411-00001  
379 bands as provided by the CDSDB and Ames line lists. According to these calculations, the evidenced  
380 interaction leads to a weak intensity transfer from the 20012-00001 band to the dark 04411-00001  
381 band around  $J= 43$ . Both calculations indicate that the strongest 04411-00001 lines, P(44) and R(42),  
382 have a predicted intensity of a few  $10^{-28} \text{ cm}^2/\text{molecule}$  which makes them detectable by high  
383 sensitivity CRDS [see *e.g.* Čermák *et al.*<sup>54</sup> and Karlovets *et al.*<sup>55</sup>]. These intensity values are six orders  
384 of magnitude smaller than the intensity of the corresponding 20012-00001 lines, illustrating the  
385 weakness of the evidenced interaction. Let us note that the level of convergence of the Ames  
386 calculations and the accuracy of the CDSDB calculations are not sufficient to account for the 15 kHz (or  
387  $5 \times 10^{-7} \text{ cm}^{-1}$ ) perturbation of the 20012  $J= 43$  level but the very faint interaction evidenced by our  
388 measurements is convincingly revealed by the intensity transfer predicted by both calculations.  
389 Although the Ames and CDSDB intensities of the 04411-00001 extra lines differ by up to 50%, the

390 agreement of the CDS and Ames predictions obtained with quite different theoretical approaches is  
 391 remarkable (**Fig. 7**). Finally, let us mention that the 20012 and 04411 states belong to the same  $P =$   
 392  $2V_1+V_2+3V_3= 7$  polyad ( $V_1$ ,  $V_2$ , and  $V_3$  are the quantum numbers of the harmonic oscillators). The  
 393 interaction mechanism is thus a  $\Delta l_2= 4$  intrapolyad interaction accounted for by the effective  
 394 Hamiltonian model used for the CDS (In fact, the original version of the CDS<sup>56</sup> was restricted to  
 395  $\Delta l_2 < 4$  bands but the  $\Delta l_2= 4$  bands were added in the updated version adopted for the HITRAN2020  
 396 line list).



397  
 398 **Fig. 7.** The 20012-00001 and the 04411-00001 bands of  $^{12}\text{CO}_2$  as provided by the CDS<sup>35</sup> and Ames<sup>53</sup>  
 399 databases. The 04411-00001 lines are induced by an intensity transfer from the 20012-00001 band for upper  $J$   
 400 values around 43.

401  
 402 From a detailed consideration of the 20012-00001 residuals presented in **Fig. 6**, it appears that  
 403 residuals associated to  $P(J+1)$  transitions are in general larger than those of the  $R(J-1)$  transitions  
 404 reaching the same  $J$  upper level. With an average difference of about 1 kHz and a similar value for the  
 405 standard deviation, the effect is small. Nevertheless, it seems to reveal some small deviations  
 406 between the  $R(J-1)$ - $P(J+1)$  ground state combination differences (GSCD) obtained from the measured  
 407 frequencies and those calculated using the ground state spectroscopic constants adopted from Wu  
 408 *et al.*<sup>10</sup>. Consequently, together with literature data, the present measurements might be valuable to  
 409 slightly refine the ground state spectroscopic constants of  $^{12}\text{CO}_2$ .

410 As main output of the present study, we provide as Supplementary Material a recommended list  
 411 of accurate  $^{12}\text{CO}_2$  transition frequencies for the 20012-00001 and 20013-00001 bands. It was  
 412 obtained as follows.

413 (i) for upper state  $J$  values smaller than 63 (e.g. P(64)-R(62) transitions), the recommended  
414 frequencies are values calculated using the spectroscopic constants of **Table 4**, except for the P(44),  
415 P(46), R(42) and R(44) perturbed transitions of the 200012-00001 band for which experimental  
416 values were kept.

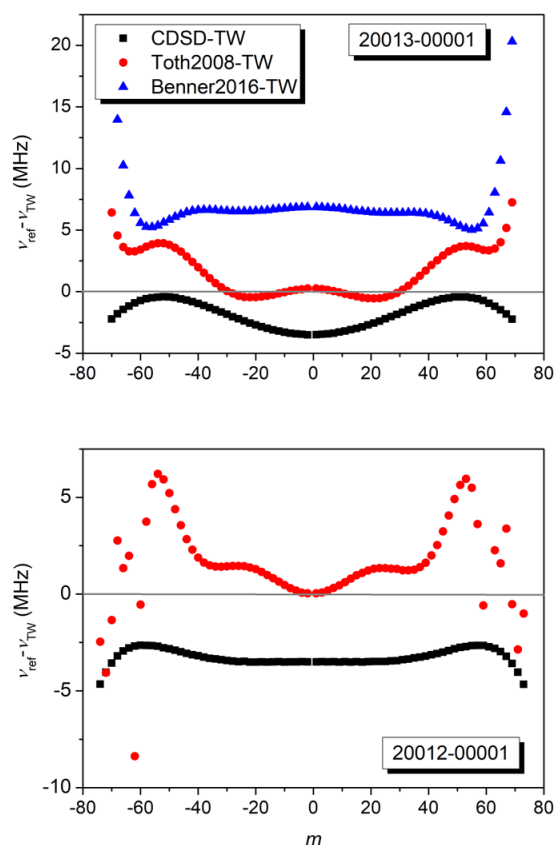
417 (ii) for  $J$  values larger than 63, experimental values are available only for R(64)-R(68) of the  
418 200012-00001 band and P(64)-P(74) of the 200012-00001 band. The experimental values were kept  
419 and complemented with their GSCD counterpart allowing extending the set of accurate frequencies  
420 beyond the observations. Finally, the recommended list, including 145 accurate transition  
421 frequencies is obtained while 107 transition frequencies were measured. This set of secondary  
422 reference standards with kHz-accuracy samples regularly the large 4788-5015  $\text{cm}^{-1}$  interval (from  
423 1994 to 2089 nm).

424 The uncertainty attached to the recommended transition frequencies derived from the fitted  
425 spectroscopic constants was obtained as the square root of the quadratic sum of the *rms* of the fit,  
426 indicated in **Table 4** for the statistical error, and of the other sources of uncertainties reported in  
427 **Table 3**.

428 The recommended frequencies can be used for comparison with literature data (**Fig. 8**). We will  
429 consider the position values included in CDS<sup>35</sup> as reproduced in the HITRAN2020 database<sup>49</sup> and  
430 measurements by Fourier transform spectroscopy (FTS) by Benner *et al.*<sup>16</sup> and Toth *et al.*<sup>21</sup>, hereafter  
431 called Benner2016 and Toth2008, respectively. For both FTS datasets, the transition frequencies are  
432 values calculated from spectroscopic constants fitted on the corresponding FTS measurements.

433 Overall, the deviations range between -4 and 7 MHz with a strong  $m$  dependence for Toth2008 ( $m$   
434 is defined as  $m = -J$  and  $m = J+1$  for  $P$  and  $R$ -branch transitions, respectively). In his publication, Toth  
435 estimated the frequency uncertainties to 1.5 MHz and 15 MHz for the strong lines and the weak high  
436  $J$  lines of strong bands, respectively. This is mostly consistent with the observations if we consider as  
437 strong lines those with  $|m| < 35$ .

438 A quite constant difference of about 6 MHz is observed for the FTS data of Benner2016, up to  $J$   
439 values of about 60. Benner *et al.* reported their positions of the 20013-00001 band with uncertainties  
440  $< 1 \times 10^{-6} \text{ cm}^{-1}$  (30 kHz) for  $0 \leq J \leq 40$ ,  $< 1 \times 10^{-5} \text{ cm}^{-1}$  for  $40 < J \leq 60$  and  $< 1 \times 10^{-4} \text{ cm}^{-1}$  for  $60 < J \leq 80$ . These  
441 values correspond to the statistical error obtained from the fit of the theoretical quantum  
442 mechanical formulae and does not include systematic errors. The evidenced 6 MHz shift (about  
443  $2 \times 10^{-4} \text{ cm}^{-1}$ ) thus measures the error of the frequency axis calibration of the used FTS spectra.



444  
 445 **Fig. 8.** Comparison between the transition frequencies reported in HITRAN2020<sup>49</sup>, derived from CDS,  
 446 Toth2008<sup>21</sup> and Benner2016<sup>16</sup> with values obtained in this work (TW) versus  $m$  for the 20012-00001 and 20013-  
 447 00001 bands. Note the different scale of the y-axis.

448 The CDS positions (adopted in HITRAN2020) are systematically lower than our values for both  
 449 bands. The CDS deviations show weak  $m$  dependence with an amplitude limited to 3.5 MHz even  
 450 for high  $J$  values, which is largely below the 300 MHz uncertainty attached to the considered  
 451 positions in the HITRAN2020 database.

452 Finally, when comparing the four frequency values reported in Mondelain *et al.*<sup>32</sup> to this work,  
 453 differences between 6 to 150 kHz are found, in agreement with the 90 kHz  $1\sigma$ -uncertainty of this  
 454 reference.

455  
 456 **5. Conclusion**

457 Frequencies of 107 transitions have been determined by saturation spectroscopy for the two  
 458 strongest bands of <sup>12</sup>CO<sub>2</sub> in the 2  $\mu$ m region which are of particular importance for remote sensing  
 459 retrievals. Compared to the most accurate literature data, the achieved kHz-accuracy represents a  
 460 gain of three orders of magnitude. These measurements, which are the first ones of the considered  
 461 bands referenced to absolute frequency reference standard, were performed by recording series of  
 462 Lamb dip spectra with a comb-referenced cavity ring down spectrometer and applying the feed-

463 forward technique *via* an electro-optic modulator to transfer the coherence of an optical comb tooth  
464 to an extended cavity laser source. The amplitude of the self-pressure shift of the Lamb-dip was  
465 evaluated for the P(60) transition of the 20012-00001 band and found significantly smaller than its  
466 usual value at higher pressure. The sub-Pa pressure values adopted for the recordings made the  
467 Lamb dip pressure shifts totally negligible in our experimental conditions.

468 The fitted values of the spectroscopic constants of the 20012 and 20013 vibrational states allow  
469 reproducing their rotational energy levels (for  $J \leq 63$ ) with an *rms* deviation of 1.1 and 0.8 kHz,  
470 respectively, the ground state spectroscopic constants being constrained to the values reported by  
471 Wu *et al.*<sup>10</sup>. A 15 kHz shift of the  $J= 43$  level of the 20012 state from its unperturbed energy value  
472 reveals a very faint interaction with a dark state. On the basis of Ames<sup>53</sup> and CDSD<sup>35</sup> theoretical  
473 calculations of the <sup>12</sup>CO<sub>2</sub> absorption spectrum, the perturber could be identified as the 04411 dark  
474 state. Interestingly, the measured 15 kHz energy shift is beyond the accuracy of both calculations but  
475 the existence of the coupling between the 20012 and 04411 states is theoretically predicted and  
476 shows up as an intensity transfer to the 04411-00001 band around the  $J= 43$  value of the energy  
477 crossing between the 20012 and 04411 states. Note that the predicted intensity of the 04411-00001  
478 extra lines are more than six orders of magnitude smaller than those of the 20012-00001.

479 Combining frequencies calculated from the determined spectroscopic constants, measurements  
480 and GSCD relations, a recommended list of 145 transition frequencies spanning the large 1.99-2.09  
481  $\mu\text{m}$  interval ( $4788\text{-}5015\text{ cm}^{-1}$ ) is provided. Most of these frequencies are given with a combined  
482 standard uncertainty on the order of 4 kHz that we believe to be conservative. They will be valuable  
483 as secondary reference standards for a number of atmospheric remote sensing.

484

#### 485 **Acknowledgements**

486 This work is funded by the European Space Agency (ESA) through the contract No.  
487 4000132228/20/I-NS with Deutsches Zentrum fuer Luft- und Raumfahrt) entitled *Improved*  
488 *Spectroscopy for Carbon Dioxide, Oxygen, and Water Vapour Satellite Measurements* for which the  
489 authors are sub-contractants. The authors are grateful to Equipex REFIMEVE+ (ANR-11-EQPX-0039)  
490 for the ultra-stable reference frequency delivered. F. Gibert from LMD and P. Cacciani from PhLAM  
491 are acknowledged for lending the Thulium doped fiber amplifier and the external cavity diode laser,  
492 respectively. The work was also supported by the joint Slovak-Czech-French Danube Region project  
493 (DS-FR-19-0050), and by the Slovak Research and Development Agency (contract number APVV-19-  
494 0386). P.C. thanks CNRS for a one-month support at LIPhy-Grenoble. DM wants to thank A. Ross  
495 from ILM and J.-M. Hartmann from LMD for fruitful discussions on global fit of effective Hamiltonians  
496 and on pressure-shifts with Lamb dips, respectively. We are indebted to X. Huang (NASA-Ames) for  
497 useful discussions about the identification of the 04411 state as perturber of the 20012 state.



- 1 D. Wunch, G. C. Toon, J. F. L. Blavier, R. A. Washenfelder, J. Notholt, B. J. Connor, D. W. T Griffith, V. Sherlock and P. O. Wennberg, The Total Carbon Column Observing Network, *Philos. T. R. Soc. A*, 2011, **369**, 2087–2112.
- 2 V. M. Devi, D. C. Benner, K. Sung, L. R. Brown, T. J. Crawford, C. E. Miller, B. J. Drouin, V. H. Payne, S. Yu, M. A. H. Smith, A. W. Mantz and R. R. Gamache, Line parameters including temperature dependences of self- and air-broadened line shapes of  $^{12}\text{C}^{16}\text{O}_2$ : 1.6- $\mu\text{m}$  region, *J. Quant. Spectrosc. Radiat. Transf.*, 2016, **177**, 117–144.
- 3 M. Birk, C. Röske and G. Wagner, High accuracy  $\text{CO}_2$  Fourier transform measurements in the range 6000–7000  $\text{cm}^{-1}$ , *J. Quant. Spectrosc. Radiat. Transf.*, 2021, **272**, 107791.
- 4 D. Mondelain, A. Campargue, H. Fleurbaey, S. Kassı and S. Vasilchenko, CRDS measurements of air-broadened lines in the 1.6  $\mu\text{m}$  band of  $^{12}\text{CO}_2$ : Line shape parameters with their temperature dependence. *J. Quant. Spectrosc. Radiat. Transf.*, 2022, **288**, 108267.
- 5 D. A. Long, S. Wójtcwicz, C. E. Miller and J. T. Hodges, Frequency-agile, rapid scanning cavity ring-down spectroscopy (FARS-CRDS) measurements of the (30012) $\leftarrow$ (00001) near-infrared carbon dioxide band, *J. Quant. Spectrosc. Radiat. Transf.*, 2015, **161**, 35–40.
- 6 R. Guo, J. Teng, H. Dong, T. Zhang, D. Li and D. Wang, Line parameters of the P-branch of (30012)  $\leftarrow$  (00001)  $^{12}\text{C}^{16}\text{O}_2$  band measured by comb-assisted, Pound-Drever-Hall locked cavity ring-down spectrometer, *J. Quant. Spectrosc. Radiat. Transf.*, 2021, **264**, 107555.
- 7 D. A. Long, G.-W. Truong, J. T. Hodges and C. E. Miller, Absolute  $^{12}\text{C}^{16}\text{O}_2$  transition frequencies at the kHz-level from 1.6 to 7.8  $\mu\text{m}$ , *J. Quant. Spectrosc. Radiat. Transf.*, 2013, **130**, 112–115.
- 8 Z. D. Reed, B. J. Drouin, D. A. Long and J. T. Hodges, Molecular transition frequencies of  $\text{CO}_2$  near 1.6  $\mu\text{m}$  with kHz-level uncertainties, *J. Quant. Spectrosc. Radiat. Transf.*, 2021, **271**, 107681.
- 9 Z. D. Reed, B. J. Drouin and J. T. Hodges, Inclusion of the recoil shift in Doppler-broadened measurements of  $\text{CO}_2$  transition frequencies, *J. Quant. Spectrosc. Radiat. Transf.*, 2021, **275**, 107885.
- 10 H. Wu, C.-L. Hu, J. Wang, Y. R. Sun, Y. Tan, A.-W. Liu and S.-M. Hu, A well-isolated vibrational state of  $\text{CO}_2$  verified by near-infrared saturated spectroscopy with kHz accuracy, *Phys. Chem. Chem. Phys.*, 2020, **22**, 2841–2848.
- 11 J. Burkart, T. Sala, D. Romanini, M. Marangoni, A. Campargue and S. Kassı, Communication: saturated  $\text{CO}_2$  absorption near 1.6  $\mu\text{m}$  for kilohertz-accuracy transition frequencies, *J. Chem. Phys.*, 2015, **142**, 191103.
- 12 Z. D. Reed, D. A. Long, H. Fleurbaey and J. T. Hodges, SI-traceable molecular transition frequency measurements at the  $10^{-12}$  relative uncertainty level, *Optica*, 2020, **7**, 1209–1220.
- 13 G.-W. Truong, D. A. Long, A. Cygan, D. Lisak, R. D. Zee and J. T. Hodges, Comb-linked, cavity ring-down spectroscopy for measurements of molecular transition frequencies at the kHz-level, *J. Chem. Phys.*, 2013, **138**, 094201.
- 14 Y. Tan, Y. R. Xu, T. P. Hua, A. W. Liu, J. Wang, Y. R. Sun and S.-M. Hu, Cavity-enhanced saturated absorption spectroscopy of the (30012)–(00001) band of  $^{12}\text{C}^{16}\text{O}_2$ , *J. Chem. Phys.*, 2022, **156**, 044201.
- 15 L. S. Rothman and L. D. Young, Infrared energy levels and intensities of carbon dioxide-II, *J. Quant. Spectrosc. Radiat. Transfer*, 1981, **25**, 505.
- 16 D. C. Benner, V. M. Devi, K. Sung, L. R. Brown, C. E. Miller, V. H. Payne, B. J. Drouin, S. Yu, T. J. Crawford, A. W. Mantz, M. A. H. Smith and R. R. Gamache, Line parameters including temperature dependences of air- and self-broadened line shapes of  $^{12}\text{C}_{16}\text{O}_2$ : 2.06- $\mu\text{m}$  region, *J. Mol. Spectrosc.*, 2016, **326**, 21–47.
- 17 R. A. Toth, L. R. Brown, C. E. Miller, V. M. Devi and D. C. Benner, Line strengths of  $^{12}\text{C}^{16}\text{O}_2$ : 4550–7000  $\text{cm}^{-1}$ . *J. Mol. Spectrosc.*, 2006, **239**, 221–242.
- 18 R. A. Toth, L. R. Brown, C. E. Miller, V. M. Devi and D. C. Benner, Self-broadened widths and shifts of  $^{12}\text{C}^{16}\text{O}_2$ : 4750–7000  $\text{cm}^{-1}$ . *J. Mol. Spectrosc.*, 2006, **239**, 243–271.
- 19 R. A. Toth, C. E. Miller, V. M. Devi, D. C. Benner and L. R. Brown, Air-broadened half width and pressure shift coefficients of  $^{12}\text{C}^{16}\text{O}_2$  bands: 4750–7000  $\text{cm}^{-1}$ , *J. Mol. Spectrosc.*, 2007, **246**, 133–157.
- 20 R. A. Toth, C. E. Miller, L. R. Brown, V. M. Devi and D. C. Benner. Line positions and strengths of  $^{16}\text{O}^{12}\text{C}^{18}\text{O}$ ,  $^{18}\text{O}^{12}\text{C}^{18}\text{O}$  and  $^{17}\text{O}^{12}\text{C}^{18}\text{O}$  between 2200 and 7000  $\text{cm}^{-1}$ , *J. Mol. Spectrosc.*, 2007, **243**, 43–61.
- 21 R. A. Toth, L. R. Brown, C. E. Miller, V. M. Devi and D. C. Benner, Spectroscopic database of  $\text{CO}_2$  line parameters: 4300–7000  $\text{cm}^{-1}$ , *J. Quant. Spectrosc. Radiat. Transf.*, 2008, **109**, 906–921.
- 22 C. B. Suarez and F. P. J. Valero, Temperature dependence of self-broadened halfwidths of  $\text{CO}_2$ . *J. Quant. Spectrosc. Radiat. Transf.*, 1990, **43**, 327–334.
- 23 L. Régalia-Jarlot, V. Zénninari, B. Parvitte, A. Grossel, X. Thomas, P. Heyden von der and G. Durry, A complete study of the line intensities of four bands of  $\text{CO}_2$  around 1.6 and 2.0  $\mu\text{m}$ : a comparison between Fourier transform and diode laser measurements, *J. Quant. Spectrosc. Radiat. Transf.*, 2006, **101**, 325–338.



- 
- 24 L. Joly, F. Gibert, B. Grouiez, A. Gossel, B. Parvitte, G. Durry and V. Zéninari, A complete study of CO<sub>2</sub> line parameters around 4845 cm<sup>-1</sup> for lidar applications, *J. Quant. Spectrosc. Radiat. Transf.*, 2008, **109**, 426–434.
- 25 L. Joly, F. Marnas, F. Gibert, D. Bruneau, B. Grouiez, P. H. Flamant, G. Durry, N. Dumelie, B. Parvitte, and V. Zéninari, Laser diode absorption spectroscopy for accurate CO<sub>2</sub> line parameters at 2 μm: consequences for space-based DIAL measurements and potential biases, *Appl. Opt.*, 2009, **48**, 5475–5483.
- 26 J. S. Li, G. Durry, J. Cousin, L. Joly, B. Parvitte, P. H. Flamant, F. Gibert and V. Zéninari, Tunable diode laser measurement of pressure-induced shift coefficients of CO<sub>2</sub> around 2.05 μm for lidar applications, *J. Quant. Spectrosc. Radiat. Transf.*, 2011, **112**, 1411–1419.
- 27 J. S. Li, G. Durry, J. Cousin, L. Joly, B. Parvitte and V. Zéninari, Self-induced pressure shift and temperature dependence measurements of CO<sub>2</sub> at 2.05 μm with a tunable diode laser spectrometer, *Spectrochim. Acta A* 2012, **85**, 74–78.
- 28 L. E. Christensen, G. D. Spiers, R. T. Menzies and J. C. Jacob, Tunable laser spectroscopy of CO<sub>2</sub> near 2.05 μm: atmospheric retrieval biases due to neglecting line-mixing, *J. Quant. Spectrosc. Radiat. Transf.*, 2012, **113**, 739–748.
- 29 G. Casa, R. Wehr, A. Castrillo, E. Fasci and L. Gianfrani, The line shape problem in the near-infrared spectrum of self-colliding CO<sub>2</sub> molecules: experimental investigation and test of semiclassical models, *J. Chem. Phys.*, 2009, **130**, 184306.
- 30 T. Q. Bui, D. A. Long, A. Cygan, V. T. Sironneau, D. W. Hogan, P. M. Rupasinghe, R. Ciuryło, D. Lisak and M. Okumura, Observations of Dicke narrowing and speed dependence in air-broadened CO<sub>2</sub> lineshapes near 2.06 μm, *J. Chem. Phys.*, 2014, **141**, 174301.
- 31 H. Fleurbaey, H. Yi, E. M. Adkins, A. J. Fleisher and J. T. Hodges, Cavity ring-down spectroscopy of CO<sub>2</sub> near λ = 2.06 μm: Accurate transition intensities for the Orbiting Carbon Observatory-2 (OCO-2) “strong band”, *J. Quant. Spectrosc. Radiat. Transf.*, 2020, **252**, 107104.
- 32 D. Mondelain, A. Campargue, H. Fleurbaey, S. Kassi and S. Vasilchenko, Line shape parameters of air-broadened <sup>12</sup>CO<sub>2</sub> transitions in the 2.0 μm region, with their temperature dependence, *J. Quant. Spectrosc. Radiat. Transf.*, 2023, **298**, 108485.
- 33 D. Gatti, N. Coluccelli, A. Gambetta, A. Di Lieto, M. Tonelli, G. Galzerano, P. Laporta and M. Marangoni, Absolute frequency spectroscopy of CO<sub>2</sub> lines at around 2.09 μm by combined use of an Er: fiber comb and a Ho: YLF amplifier, *Opt. Lett.*, 2011, **36**, 3921–3923.
- 34 F. Gibert, D. Edouart, P. Monnier, C. Cénac, J. López and J. Collignan, A wind, temperature, H<sub>2</sub>O and CO<sub>2</sub> scanning lidars mobile observatory to study surface- atmosphere interaction. Application in temperate and semi-arid region, *European Lidar Conference (ELC2021)*, Nov 2021, Granada, Spain.
- 35 S. A. Tashkun, V. I. Perevalov, R. R. Gamache and J. Lamouroux, CDS-296, high-resolution carbon dioxide spectroscopic databank: An update, *J. Quant. Spectrosc. Radiat. Transf.*, 2019, **228**, 124–131.
- 36 Laser Spectroscopy: Vol. 2: Experimental Techniques 4th Edition by Wolfgang Demtröder (Author) , Springer Ed.
- 37 G. Giusfredi, S. Bartalini, S. Borri, P. Cancio, I. Galli, D. Mazzotti and P. De Natale, Saturated-absorption cavity ring-down spectroscopy, *Phys. Rev. Lett.*, 2010, **104**, 1–4.
- 38 J. Wang, Y. R. Sun, L.-G. Tao, A.-W. Liu, T.-P. Hua, F. Meng and S.-M. Hu, Comb-locked cavity ring-down saturation spectroscopy, *Rev. Sci. Instrum.*, 2017, **88**, 043108.
- 39 S. Vasilchenko, T. Delahaye, S. Kassi, A. Campargue, R. Armante, H. Tran and D. Mondelain, Temperature dependence of the absorption of the R (6) manifold of the 2ν<sub>3</sub> band of methane in air in support of the MERLIN mission, *J. Quant. Spectrosc. Radiat. Transf.*, 2023, **298**, 108483.
- 40 O. Votava, S. Kassi, A. Campargue and D. Romanini, Comb coherence-transfer and cavity ring-down saturation spectroscopy around 1.65 μm: kHz-accurate frequencies of transitions in the 2ν<sub>3</sub> band of <sup>12</sup>CH<sub>4</sub>, *Phys. Chem. Chem. Phys.*, 2022, **24**, 4157–4173.
- 41 R. Gotti, M. Prevedelli, S. Kassi, M. Marangoni and D. Romanini, Feed-forward coherent link from a comb to a diode laser: Application to widely tunable cavity ring-down spectroscopy, *J. Chem. Phys.*, 2018, **148**, 054202.
- 42 <https://www.refimeve.fr/index.php/en/>
- 43 J. Burkart. (2015). Optical feedback frequency-stabilized cavity ring-down spectroscopy - Highly coherent near-infrared laser sources and metrological applications in molecular absorption spectroscopy. PhD Thesis.
- 44 D. Romanini, P. Dupré and R Jost, Non-linear effects by continuous wave cavity ringdown spectroscopy in jet-cooled NO<sub>2</sub>, *Vibrational Spectroscopy*, 1999, **19**, 93–106.
- 45 S. Kassi, T. Stoltmann, M. Casado, M. Daëron, and A. Campargue, Lamb dip CRDS of highly saturated transitions of water near 1.4 μm, *J. Chem. Phys.*, 2018, **148**, 054201.

- 
- 46 V. A. Alekseev, T. L. Andreeva and I. I. Sobelman, Contribution to the theory of nonlinear power resonances in gas lasers, *Sov. Phys.-JETP*, 1973, **37**, 413-418.
- 47 S. Bagaev, E. Baklanov and V. Chebotaev, Anomalous decrease of the shift of the center of the Lamb dip in low-pressure molecular gases, *Sov. J. Exp. Theor. Phys. Lett.*, 1972, **16**, 243.
- 48 V. S. Letokhov, (1976). Saturation spectroscopy. In: Shimoda, K. (eds) High-Resolution Laser Spectroscopy. Topics in Applied Physics, vol 13. Springer, Berlin, Heidelberg.
- 49 I. E. Gordon, L. S. Rothman, R. J. Hargreaves, R. Hashemi, E. V. Karlovets, F. M. Skinner, E. K. Conway, C. Hill, R. V. Kochanov, Y. Tan, P. Wcisło, A. A. Finenko, K. Nelson, P. F. Bernath, M. Birk, V. Boudon, A. Campargue, K. V. Chance, A. Coustenis, B. J. Drouin, J.-M. Flaud, R. R. Gamache, J. T. Hodges, D. Jacquemart, E. J. Mlawer, A. V. Nikitin, V. I. Perevalov, M. Rotger, J. Tennyson, G. C. Toon, H. Tran, V. G. Tyuterev, E. M. Adkins, A. Baker, A. Barbe, E. Canè, A. G. Császár, A. Dudaryonok, O. Egorov, A. J. Fleisher, H. Fleurbaey, A. Foltynowicz, T. Furtenbacher, J. J. Harrison, J.-M. Hartmann, V.-M. Horneman, X. Huang, T. Karman, J. Karns, S. Kassi, I. Kleiner, V. Kofman, F. Kwabia-Tchana, N. N. Lavrentieva, T. J. Lee, D. A. Long, A. A. Lukashetskaya, O. M. Lyulin, V. Y. Makhnev, W. Matt, S. T. Massie, M. Melosso, S. N. Mikhailenko, D. Mondelain, H. S. P. Müller, O. V. Naumenko, A. Perrin, O. L. Polyansky, E. Raddaoui, P. L. Raston, Z. D. Reed, M. Rey, C. Richard, R. Tóbiás, I. Sadiek, D. W. Schwenke, E. Starikova, K. Sung, F. Tamassia, S. A. Tashkun, J. Vander Auwera, I. A. Vasilenko, A. A. Viganin, G. L. Villanueva, B. Vispoel, B. G. Wagner, A. Yachmenev and S. N. Yurchenko, The HITRAN2020 molecular spectroscopic database, *J. Quant. Spectrosc. Radiat. Transf.*, 2022, **277**, 107949.
- 50 C. Boulet. Personal communication.
- 51 W. Q. Cai, T. E. Gough, X. J. Gu, N. R. Isenor and G. Scoles, Polarizability of CO<sub>2</sub> studies in molecular beam laser Stark spectroscopy, *Phys. Rev. Lett.*, 1987, **36**, 4722.
- 52 L. A. Rahn, R. L. Farrow, M. Koszykowski and P. Mattern, *Phys. Rev. Lett.*, 1980, **45**, 620.
- 53 X. Huang, D. W. Schwenke, R. S. Freedman and T. J. Lee, Ames-2016 line lists for 13 isotopologues of CO<sub>2</sub>: Updates, consistency, and remaining issues, *J. Quant. Spectrosc. Radiat. Transf.*, 2017, **203**, 224-241.
- 54 P. Čermák, E. V. Karlovets, D. Mondelain, S. Kassi, V. I. Perevalov and A. Campargue, High sensitivity CRDS of CO<sub>2</sub> in the 1.74 μm transparency window. A validation test for the spectroscopic databases, *J. Quant. Spectrosc. Radiat. Transf.*, 2018, **207**, 95-103.
- 55 E.V. Karlovets, S. Kassi and A. Campargue, High sensitivity CRDS of CO<sub>2</sub> in the 1.18 μm transparency window. Validation tests of current spectroscopic databases, *J. Quant. Spectrosc. Radiat. Transf.*, 2020, **247**, 106942.
- 56 S. A. Tashkun, V. I. Perevalov, R. R. Gamache and J. Lamouroux, CDSD-296, high resolution carbon dioxide spectroscopic databank: Version for atmospheric applications, *J. Quant. Spectrosc. Radiat. Transf.*, 2015, **152**, 45-73.